

Synthesis and characterization of $\text{Sc}_2\text{Mo}_3\text{O}_{12}:\text{Yb}^{3+}/\text{Er}^{3+}$

A Dissertation for
PHY-651:Dissertation
Credits: 16

Submitted in partial fulfilment of Masters degree in Physics
By

VAIBHAV VITHU CHARI

Seat Number: 22PO430044

ABC ID: 874001881121

PRN: 201802574

Under the Supervision of

VENKATESH R HATHWAR

School of Physical and Applied Sciences



GOA UNIVERSITY
MAY 2024

Examined by:



Seal of the School

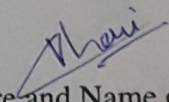
DECLARATION BY STUDENT

I hereby declare that the data presented in this Dissertation report entitled, "**Synthesis and characterization of $\text{Sc}_2\text{Mo}_3\text{O}_{12}:\text{Yb}^{3+}/\text{Er}^{3+}$** " This is based on the results of investigations carried out by me in the Masters of Physics at the School of Physical and Applied Science, Goa University, under the Supervision of UGC Assistant Prof. Dr Venkatesha R. Hathwar. I have not submitted the same elsewhere for a degree or diploma award. Further, I understand that Goa University or its authorities will not be responsible for the correctness of observations / experimental or other findings given the dissertation.

I hereby authorize the University authorities to upload this dissertation to the dissertation repository or anywhere else as the UGC regulations demand and make it available to anyone as needed.

Date: 2 May 2024

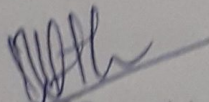
Place: Goa University


Signature and Name of Student

Seat no : 22PO430044

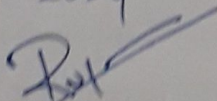
COMPLETION CERTIFICATE

This is to certify that the dissertation report "Synthesis and characterization of $\text{Sc}_2\text{Mo}_3\text{O}_{12}:\text{Yb}^{3+}/\text{Er}^{3+}$ " is a bonafide work carried out by Mr. Vaibhav Vithu Chari under my supervision in partial fulfilment of the requirements for the award of the degree of Master of Science in Physics at the School of Physical and Applied Science, Goa University.



Signature of Supervising Teacher

Date: 09-05-2024



Signature of Dean of the School

Date:

Place: Goa University



School stamp

ACKNOWLEDGEMENT

I am pleased to present the report of my project work undertaken during my M.Sc. final year. Although I worked hard for the success of this project, it would not have been possible without the help and guidance of some people. Therefore, I would like to express my deep gratitude to those individuals.

Firstly, I would like to thank my project guide, Dr Venkatesha R. Hathwar, for his excellent guidance and intelligence. Thank you, sir, for always motivating and inspiring me. Secondly, I would like to thank Mr. Mahendra Chaudhary for his constant help and support throughout the project. Thank you so much, sir, for being a great guide and friend. Thirdly, I want to acknowledge all the PhD students in the physics department who have assisted me by explaining how to use different instruments and software.

Next, I want to thank the School of Physical and Applied Sciences for providing me with all the required instruments for my project work. Next, I want to thank other faculties of physics for providing me with the conceptual knowledge needed. I want to express my gratitude towards my parents for their kind encouragement and appreciation throughout.

TABLES AND FIGURES

List of Figures

1	Energy level Scheme of the luminescent ion A. The A* indicates the excited state, R the radiative return, and NR the nonradiative return to the ground state.	2
2	Types of Luminescence	4
3	Electronic configurations of trivalent rare-earth ions in the ground state	7
4	Conversion of NIR to VIS by UCNF	9
5	Energy levels of Er^{3+} ion	12
6	Hydrothermal synthesis process	24
7	Schematic representation of Bragg's Law	30
8	Formation of the cone of the diffracted beam.	31
9	Rigaku Smart Lab Powder X-ray diffractometer at ULMC of Goa University	32
10	Rigaku Smart Lab Powder X-ray diffractometer at ULMC of Goa University	33
11	Schematic diagram of a Scanning electron microscope	34
12	Carl Zeiss Scanning Electron Microscope at ULMC of Goa University	36
13	XRD plot of both samples	37
14	$\text{Sc}_{1.6}\text{Mo}_3\text{O}_{12} : 0.36\text{Yb}^{3+} : 0.04\text{Er}^{3+}$	38
15	$\text{Sc}_{1.42}\text{Mo}_3\text{O}_{12} : 0.54\text{Yb}^{3+} : 0.04\text{Er}^{3+}$ refinement	38

16	$\text{Sc}_{1.42}\text{Mo}_3\text{O}_{12} : 0.54\text{Yb}^{3+} : 0.04\text{Er}^{3+}$	39
17	$\text{Sc}_{1.6}\text{Mo}_3\text{O}_{12} : 0.36\text{Yb}^{3+} : 0.04\text{Er}^{3+}$	39
18	Graph of Absorbance vs Wavelength.	40
19	UV recording spectrometer and degraded MO	40
20	Graph of Ct/Co vs Time for $\text{Sc}_{1.42}\text{Mo}_3\text{O}_{12} : 0.54\text{Yb}^{3+} : 0.04\text{Er}^{3+}$.	41
21	Graph of $-\ln(\text{Ct/Co})$ vs Time for $\text{Sc}_{1.42}\text{Mo}_3\text{O}_{12} : 0.54\text{Yb}^{3+} :$ 0.04Er^{3+}	41

List of Tables

1	Chemical Formulas and their Masses	25
2	Chemical Formulas and their Masses	25
3	Lattice parameters for samples.	39

ABBREVIATIONS USED

Entity	Abbreviation
SEM	Scaning Electron Microscope
NTE	Negative Thermal Expansion
MO	Methyl Orange
XRD	X-Ray Diffraction

ABSTRACT

This study presents an analysis of $\text{Sc}_2\text{Mo}_3\text{O}_{12}$ with 2 dopant coconcentrations of Yb and Er (18% , 27% and 2% respectively) using XRD refinement and SEM analysis. The powder XRD data was obtained from finely ground samples at ULMC at Goa University. Both compounds were found to be orthorhombic in nature as per the PXRD analysis. The SEM images revealed an irregular topography of the samples with sizes ranging from 2 to 8 microns. Furthermore, the compound $\text{Sc}_{1.42}\text{Mo}_3\text{O}_{12} : 0.54\text{Yb}^{3+} : 0.04\text{Er}^{3+}$ was used as a photocatalyst for the degradation of Methyl Orange. The degradation process was monitored over a period of 120 minutes, and the slope of the graph of $-\ln(\text{Ct}/\text{Co})$ vs Time gave a degradation constant value of 0.984.

Contents

1	Luminescence	1
1.1	General characteristics of luminescence	2
1.2	Extrinsic luminescence	3
1.3	Rare earth elements and their properties	4
1.4	Upconversion luminescence	8
1.4.1	Energy transfer mechanisms in upconversion luminescence	9
1.4.2	Role of host, activator and sensitizer in UC mechanism . .	11
1.4.3	Activators	11
1.4.4	Sensitizer	12
1.5	Negative Thermal Expansion	14
1.5.1	Introduction	14
1.5.2	Negative thermal expansion in $A_2M_3O_{12}$	16
1.5.3	Mechanism of NTE	18
1.5.4	Non-Hygroscopic	19
2	Review about $Sc_2Mo_3O_{12}$	21
2.1	$A_2M_3O_{12}$ Family of Materials	21
2.2	Effect of A-site Cation on Properties	22
2.3	Introduction to Methyl Orange Degradation	22
2.3.1	Mechanisms of UV Light-Assisted Degradation	23
2.3.2	Factors Influencing the Degradation Process	23
3	Hydrothermal synthesis of $Sc_2Mo_3O_{12}$	24
3.1	Procedure	24

3.2	List of chemicals	25
3.3	Procedure for Degradation of Methyl orange	26
3.4	Procedure for XRD refinement	26
4	Characterisation of $\text{Sc}_2\text{Mo}_3\text{O}_{12}$	28
4.1	X-ray diffraction	28
4.1.1	Generation of X-rays	28
4.1.2	Interaction of X-rays with matter	29
4.2	Powder XRD method	30
4.2.1	Powder X-ray Diffractometer	31
4.3	Scanning Electron Microscopy	33
4.3.1	Principle	33
4.3.2	Instrumentation	35
4.3.3	Application	35
5	Analysis of $\text{Sc}_2\text{Mo}_3\text{O}_{12}$	37
5.1	XRD Refinement	37
5.2	SEM analysis	39
5.3	UV degradation	39

CHAPTER 1 *INTRODUCTION*

1 Luminescence

Among the scientific disciplines that potentially fuel advancements in both science and technology, luminosity is one of the fastest growing. Due to the distinct requirements of life sciences and display technology, luminescence-based technology has grown rapidly during the last ten years. Despite knowing that luminescence is a historic phenomenon, the area remains ever-growing and excited, with many new materials and discoveries being made. When an excitation stops, luminescence, which is light released by a substance which is brighter than blackbody radiation, continues to exist throughout the duration of electromagnetic energy in the visible spectrum. The material that glows is known as phosphor.[7] The initial studies of luminous crystals took place in the twentieth century by Lenard and his school. "Leonard phosphorus" is the name of the phosphorous they are now studying.

Research on crystalline luminescence was significantly aided by interest in luminous minerals used in high-efficiency cathode ray displays and, afterwards, the creation of the luminescent lamp in the early 1930s.[14]

Luminescence, in general, relates to light emissions that are not primarily thermal in origin. Within the field of luminescence, two primary generalizations could be made: Interest in luminescent materials used in high-efficiency cathode ray displays and, eventually, the luminescent lamp developed in the 1930s greatly stimulated research on crystalline luminescence.[16]

Generally speaking, luminous emissions that are not purely thermal in origin

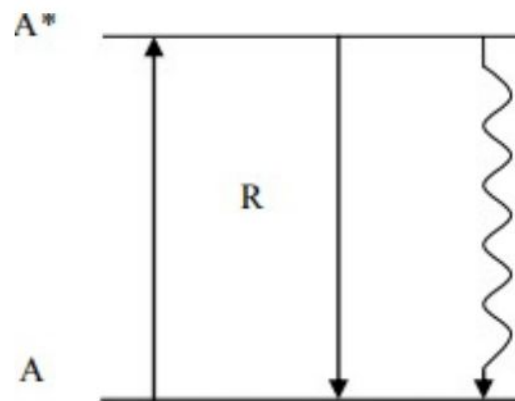


Figure 1: Energy level Scheme of the luminescent ion A. The A^* indicates the excited state, R the radiative return, and NR the nonradiative return to the ground state.

are included in the term luminescence. In the field of luminescence, there are two major generalizations:

Exciting an electron to a high-energy band, leaves a positive hole in a lower band, which can recombine to give luminescence emission. An excited electron may lose its energy immediately or after a period of time by emitting radiation. Two or more steps may result in loss of power, any of which could lead to the emission of a visible photon. The substances that produce delayed visible radiation after suitable external excitation are called phosphors.[12]

1.1 General characteristics of luminescence

The process of luminescence can be illustrated in figure below.

Radiative and nonradiative return to the ground state is shown in the figure. This is in the latter case where the process of luminescence begins. The other, which is brought about by radiative emission of phonons that are converted into lattice vibrations that carry energy in the form of heat, is not connected to luminescence. vibrations that carry heat energy throughout them. If radiative transitions dominate nonradiative ones in a luminescent material, it is regarded as efficient.

The promoting radiation is absorbed elsewhere and is not absorbed by the activator, although the fact that the situation with luminescent materials is more complex than it seems in the image that precedes. The duration of the emission defines another type of luminescence.[4]

- **Fluorescence:** An exponential afterglow is seen upon removal of excitation, which is independent of temperature and excitement intensity and with a lifetime of less than 10^{-8} seconds.
- **Phosphorescence:** Another events known as afterglow, which has a lifetime of more than 10^{-8} seconds and decays progressively with complex dynamics, appears upon removal of excitation. It frequently depends on the intensity of excitation and significantly temperature-dependent. This effect could be caused by metastable states that are generated by the activators, electron or hole traps, defect centers, and impurities in the lattice, which would postpone the bright emission. Because emission won't happen until the metastable activator or trap has been successfully thermally triggered.

1.2 Extrinsic luminescence

Extrinsic light is the luminescence that occurs by intentionally adding defects or impurities to the phosphor. It could be either localized or unlocalized in instances of semiconductors and ion crystals. If the luminescence is additionally triggered by free holes in the valence band and free electrons in the conduction band of the host lattice, than it is unlocalized. On the other hand, this localized create occurs when there is a limit in the luminescence's excitation and emission processes.[14, 16]

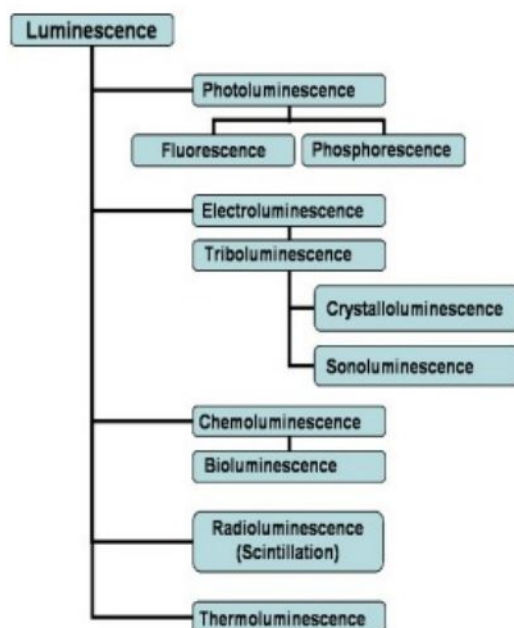


Figure 2: Types of Luminescence

1.3 Rare earth elements and their properties

The lanthanide series includes elements from lanthanum (La, $Z = 57$) to lutetium (Lu, $Z = 71$). The term 'rare earth' traditionally refers to a group of elements that includes the lanthanides, along with scandium (Sc) and yttrium (Y). Each new element discovered in the rare earth portfolio posed a different problem for Mendeleev. This was because it proved difficult to place them in his periodic table because of their very comparable chemical properties. The completely full $5s^2$ and $5p^6$ orbitals are responsible for sheltering the $4f$ valence electrons, thereby accounting for these chemical similarities. Each element in this family has distinctive physical features such as color, luminescence, which and nuclear magnetic qualities, despite their equivalent chemical composition. The elements themselves are not rare, but the minerals (cerite and gadolinite) in which they first appeared are. For instance, the most common member of the family, cerium (Ce), is iden-

tical to tin in that it exists in the earth's crust at 66 parts every million. Even the least frequent lanthanide, thulium (Tm), is far more prevalent than silver or cadmium

Lanthanides are becoming increasingly crucial to today's environment, particularly for applications which involve light emission. The great color purity of lanthanides is one of its primary advantages. The fact that trivalent lanthanide ions exhibit unique electronic transitions in the visible, near-infrared, and ultraviolet spectrum areas.

- **Magnetic Properties** — Certain rare earth elements, such Dy, Sm, and Nd, have been appreciated for their magnetic properties. When unpaired electrons spin in the same direction, these elements align and produce magnetic fields. As a result, these materials have a large magnetic storage of energy capability. Rare earth magnets are utilized extensively in numerous different fields, such as missile and airplane guiding systems and wind turbines.
- **Electrical Properties** — The elements of rare earths are capable of being employed in nickel-metal hydride (NiMH) batteries due to its electrical nature. These batteries' anodes are composed of mischmetal, which is a mixture of praseodymium, neodymium, lanthanum, and cerium. Since the rare earth metals are not required to be fully separated, this composition is inexpensive. These elements increase the energy storage capacity of the batteries per unit weight and enhance their ability to last throughout numerous cycles of discharge and recharge.
- **Catalytic Properties** — Rare earths may initiate chemical reactions due to its electron structure. As cerium and lanthanum are plentiful and inexpen-

sive, they are primarily used for catalytic applications. Whereas lanthanum is frequently utilized in fluid catalytic cracking, a technique that converts crude oil into specific functional hydrocarbons such as gasoline, cerium is used in catalytic converters for gasoline-powered automobiles.

- **Luminescent Properties** — Several rare earth elements, when activated by electromagnetic radiation, release light. Energy-efficient light sources like LEDs and compact fluorescent bulbs utilize these elements as phosphors. Red-light-emitting europium phosphors played a key role in the 1960s development of color television. Signals transmitted through glass fibers can be enhanced thanks to erbium ion fluorescent properties. Another use for the luminous qualities of certain rare earths is in lasers. For solid-state lasers, yttrium-aluminum-garnet (YAG) is a typical medium. YAG lasers doped with erbium generate focused light wavelengths, which are helpful in dentistry and oral surgery. YAG lasers are utilized extensively in manufacturing, healthcare, and military applications when doped with neodymium. .

According to the electronic configuration, Sc^{3+} corresponds to Ar, Y^{3+} to Kr, and La^{3+} to Xe. The lanthanides from Ce^{3+} to Lu^{3+} incorporate one to fourteen 4f electrons in their inner shell configuration, which is equivalent to Xe. Ions devoid of 4f electrons, i.e., Sc^{3+} , Y^{3+} , La^{3+} , and Lu^{3+} , lack electronic energy levels that can induce excitation and luminescence processes in or near the visible region. In contrast, the ions from Ce^{3+} to Yb^{3+} , which have partially filled 4f orbitals, possess energy levels characteristic of each ion and exhibit a range of luminescence properties around the visible region.

The azimuthal quantum number (l) of the 4f orbitals is 3, leading to 7 ($= 2l+1$) orbitals, each capable of accommodating two electrons. In the ground state, elec-

Atomic Number	Ions	Corresponding element	4f electron	S	L	J
				Σs	Σl	$\Sigma(L+S)$
21	Sc ³⁺	Ar		0	0	0
39	Y ³⁺	Kr		0	0	0
57	La ³⁺			0	0	0
58	Ce ³⁺	Xe	↑	1/2	3	5/2
59	Pr ³⁺	Xe	↑↑	1	5	4
60	Nd ³⁺	Xe	↑↑↑	3/2	6	9/2
61	Pm ³⁺	Xe	↑↑↑↑	2	6	4
62	Sm ³⁺	Xe	↑↑↑↑↑	5/2	5	5/2
63	Eu ³⁺	Xe	↑↑↑↑↑↑	3	3	0
64	Gd ³⁺	Xe	↑↑↑↑↑↑↑	7/2	0	7/2
65	Tb ³⁺	Xe	↑↓↑↑↑↑↑↑	3	3	6
66	Dy ³⁺	Xe	↑↓↑↓↑↑↑↑↑↑	5/2	5	15/2
67	Ho ³⁺	Xe	↑↓↑↓↑↓↑↑↑↑↑↑	2	6	8
68	Er ³⁺	Xe	↑↓↑↓↑↓↑↓↑↑↑↑↑↑	3/2	6	15/2
69	Tm ³⁺	Xe	↑↓↑↓↑↓↑↓↑↓↑↑↑↑↑↑	1	5	6
70	Yb ³⁺	Xe	↑↓↑↓↑↓↑↓↑↓↑↓↑↑↑↑↑↑	1/2	3	7/2
71	Lu ³⁺	Xe	↑↓↑↓↑↓↑↓↑↓↑↓↑↓↑↓↑↓↑↓	0	0	0

Figure 3: Electronic configurations of trivalent rare-earth ions in the ground state

trons are distributed to provide the maximum combined spin angular momentum S . The spin angular momentum s is further combined with the orbital angular momentum (L) to produce the total angular momentum (J) as follows: $J = L - S$, when the number of 4f electrons is less than 7, and $J = L + S$, when the number of 4f electrons is greater than 7.

The electronic state is indicated by the notation $2S + 1LJ$, where L represents S,P,D,F,G,H, I, K,L,M, corresponding to $L = 0, 1, 2, 3, 4, 5, 6, 7, 8, 9$, respectively. More accurately, as an intermediate coupling state, which can be described as a mixed state of several $2S + 1LJ$ states combined by spin-orbit interaction. However, for qualitative discussions, the principal L state can be taken to represent the actual state. The mixing resulting from spin-orbit interaction is small for the levels near ground states, while it is considerable for excited states that have neighboring states with similar J numbers. The effect of mixing is relatively small on the energy of levels, but can be large on their optical transition probabilities.

These transitions are intra-configurational 4f-4f transitions. Typically, a lanthanide ion's spectrum exhibits two distinct kinds of transitions. Since most of the transitions are induced electric dipole transitions (ED), which only happen within a single (4f) configuration, they are forbidden by the Laporte selection criterion. Magnetic dipole transitions (MD) are one type of transition. The transitions aren't particularly strong regardless of the situation. The environment in which the trivalent lanthanide ion exists in has very little effect on the 4f shell due to the filled 5s and 5p shells' rather effective shielding. As a result, rather than the wide bands that are common for transition metals, the transitions appear as sharp lines. Additionally, this causes the excited state to decay more slowly, hence why trivalent lanthanides exhibit intense luminosity..

The luminescent properties of the lanthanides have also been utilized in medical diagnosis. A variety of sensors have been developed that take advantage of the unique luminescent properties of these elements, such as a relatively long-lived emission of lanthanides.

1.4 Upconversion luminescence

The luminescence conversion process in materials doped with lanthanides involves the absorption of long-wavelength radiation and the subsequent emission of short-wavelength radiation. This process essentially transforms low-energy incident light, typically in the infrared (IR) region, into higher-energy light such as visible (Vis), ultraviolet (UV), or near-infrared light (NIR). This nonlinear optical phenomenon is known as anti-Stokes emission.

The remarkable signal-to-noise ratio of lanthanide-doped nanoparticles, which

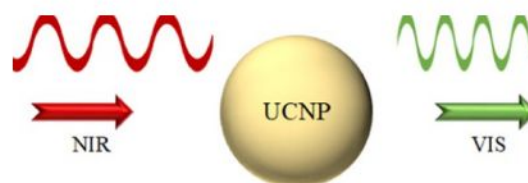


Figure 4: Conversion of NIR to VIS by UCNP

raises detection sensitivity, is one of its intrinsic features. The primary cause of this is the decreased autofluorescence in the 700–1100 nm NIR diagnostic range. These materials also have high anti-Stokes shift, good chemical and photostability, and narrow emission peaks, along with other special characteristics.

1.4.1 Energy transfer mechanisms in upconversion luminescence

UC luminescent process is a complex process of various processes in essence, excited-state absorption (ESA), energy transfer upconversion (ETU), cooperative upconversion, cross-relaxation (CR), photon avalanche (PA), and energy migration-mediated upconversion (EMU).

- **Ground State Absorption (GSA)** is the process that takes place when a single ion combines with incident photons and electrons for an extended period of time, stimulating the electrons and photons from their ground state to an excited state. The energized State Absorption (ESA) mechanism describes how the electrons at the metastable state interact with a different pump photon to be triggered to a higher excited state. Through a sequence of procedures, these ions are gradually stimulated to the Upconversion (UC) luminous state. A UC photon emerges when the electrons in the UC state radiate back to the ground state after a period of relaxation.

To achieve high UC luminescent efficiency of GSA/ESA, the energy structure of the activator should resemble a ladder-like or stepwise structure with nearly uniformly spaced energy levels of Ln^{3+} ions. However, only a limited number of lanthanides (Ho^{3+} , Er^{3+} , Tm^{3+} , and Nd^{3+}) can exhibit such energy level structures that are suitable for the GSA/ESA process to achieve UC luminescence. The GSA/ESA mechanism requires only one type of dopant and activator, which are independent of the ion-ion distance. However, this process can only achieve low UC efficiency due to the small absorption cross section of these elements (Ho^{3+} , Er^{3+} , Tm^{3+} , and Nd^{3+}).

- **Energy Transfer Upconversion (ETU)** requires the presence of two distinct types of neighboring ions: an activator (Ion II) with multiple Upconversion (UC) luminescence capabilities and a sensitizer (Ion I) with a high absorption cross-section. Through the absorption of incoming photons, the sensitizer (Ion I) in the ETU process is first stimulated from its ground state to a metastable state. The ion is then stimulated to its higher emission state as a result of the electrons in the sensitizer's metastable state relaxing back to the ground state and passing energy to the nearby ion (activator (Ion II)).

The average distance between neighboring sensitizer activators, which is determined by the concentration of dopant, affects the UC luminescence efficiency of the ETU process. Excited State Absorption (ESA), on the contrary, is a single ion distinctive whose efficiency is independent of dopant concentration.

The electrochemical transformation (ETU) is recognized as the most effi-

cient procedure for lanthanide upconversion. The most common combinations of sensitizer-activator that exhibit high brightness are $\text{Yb}^{3+}/\text{Er}^{3+}$, Ho^{3+} , Tm^{3+} with an excitation wavelength of approximately 980 nm, and $\text{Nd}^{3+}/\text{Yb}^{3+}/\text{Er}^{3+}$, Ho^{3+} , Tm^{3+} with excitation wavelengths of approximately 980 nm and 808 nm.

1.4.2 Role of host, activator and sensitizer in UC mechanism

A key consideration in the development of Upconversion Nanoparticles (UCNPs) is the selection of the host material, which determines key UC characteristics such as photon UC efficiency and visible emission spectra. Radiation is released when the sensitizer, which is easily triggered to higher levels by an incident photon of light, transfers its energy to the activator. As a result, the activator plays an essential role in the UC process as a luminescence center. Dopant concentrations in the host lattice are typically rather low, with the emitter typically being 2 mol -% and the absorber typically being 20 mol%.

1.4.3 Activators

Due to their long excited-state lifetimes and the availability of ladder-like energy levels, Er^{3+} , Tm^{3+} , Nd^{3+} , Pr^{3+} , and Ho^{3+} are effective activator ions for upconversion luminescence. Theoretically, all lanthanide ions are anticipated to exhibit Upconversion Luminescence (UCL) owing to their long-lived excited states. For practical UCL generation, the energy difference between each excited level and the lower lying level should be within the Near-Infrared (NIR) range to facilitate upconversion.

Er^{3+} has an exceptional upconversion efficiency since the energy gap between its

various energy levels are the same. The energy difference between $4I_{11/2}$ and $4I_{15/2}$ (10350 cm^{-1}) corresponds to that between $4F_{7/2}$ and $4I_{11/2}$ (10370 cm^{-1}), as Figure 1.4, the energy level diagram of Er^{3+} , illustrates. In the same region, there is a difference between $4F_{9/2}$ and $4I_{13/2}$. Thus, emission in the green and red regions can be attributed to at least three transitions in Er^{3+} that may be caused by 980 nm excitation. UCL emission results from this transition between the Er levels ($4I_{15/2}$, $4F_{7/2}$, $4I_{11/2}$) using 980 nm excitation.

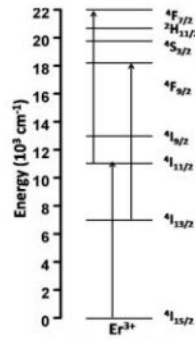


Figure 5: Energy levels of Er^{3+} ion

1.4.4 Sensitizer

Cross relaxation sets a constraint on the activator's concentration. Therefore, to enhance the effective absorption of the excitation photon, sensitizers are needed, ions that have excellent absorption that can be co-doped with activator ions. Sensitized luminescence is the term used to describe Upconversion Luminescence (UCL), in which an ion with a high Near-Infrared (NIR) absorption cross-section is co-doped with the activator to boost the luminescence intensity. Energy Transfer Upconversion (ETU) is the method through which the photon absorbed by the sensitizer is transferred to the activator. . Due to its simple energy level structure, which has a single excited state at 980 nm above the ground state, Yb^{3+} is

a widely used sensitizer. Because there is a lower possibility of cross-relaxation here, the sensitizer is going to have a higher doping concentration than the activator. The ETU in an Er^{3+} - Yb^{3+} co-doped system is shown in Figure 1.6. The energy absorbed by Yb^{3+} is transferred to Er^{3+} levels, as the image shows. Through non-radiative relaxation and cross-relaxation, the green ($2H_{11/2}$, $4S_{3/2}$) and red ($4F_{9/2}$) emitting levels of Er^{3+} were populated. By altering the Yb material, the material's luminescence emission color will change according to the intensity ratio between the two emissions.

1.5 Negative Thermal Expansion

1.5.1 Introduction

Thermal expansion refers to the alteration in the dimensions of a substance due to a change in temperature. It characterizes the propensity of solid entities to augment in length or volume when subjected to heat. This phenomenon is typically observed for macroscopic alterations in substances, but can also be discerned at the atomic scale. Thermal expansion is usually quantified [3] extensively to determine macroscopic changes in the substance, but can also be quantified at the atomic level through intrinsic methodologies. At the atomic scale, thermal expansion is frequently characterized as bond elongation, and is discerned when vibrational modes lead to an augmentation in interatomic distances.[17]

This pattern is best elucidated through comprehension of the asymmetric form of a typical interatomic potential well for longitudinal oscillations between two atoms. As higher energy vibrational states are populated, extended interatomic distances become preferable[6, 8, 1].

Thermal expansion is characterized by the expansion coefficient α , which delineates the magnitude of thermal expansion a substance will exhibit. In a solid or liquid, a dynamic equilibrium exists between the cohesive forces that hold the atoms or molecules together, and vibration. Consequently, a material's thermal expansion depends on the strength of the atomic bonds, as well as the influence of temperature, that induces thermal vibrations sufficient for atom separation. Therefore, increased distances between neighboring atoms are typically the result of heating[8].

For more intricate materials, other vibrations can contribute or even predominate the macroscopic expansion behavior. Longitudinal vibrations will still lead to bond expansion on a localized scale, but transverse vibrational modes may lead to the contrary effect on a unit cell scale. These competing effects can result in zero, positive, or negative thermal expansion. These three categories of thermal expansion are governed by the dimensional changes observed in each case. Upon heating, most solids increase in size or undergo positive thermal expansion. Materials that exhibit zero thermal expansion show no dimensional changes when heated. There are rare circumstances that may cause a decrease in the dimensions of a solid over a certain temperature range. This phenomenon is known as negative thermal expansion[10].

Materials have distinctive bonding arrangements and forces, which results in unique expansion coefficients. In applications where the system's temperature is varied, some degree of thermal expansion is usually observed. Regrettably, issues may arise if several materials are bonded that have significantly different α values. For instance, thermal stresses and strains at an interface that result from differences in thermal expansion or contraction can be detrimental to metallurgical applications at elevated temperatures. In other applications, stresses, cracks, or separation at the interface can occur between materials with mismatched thermal expansion. These effects may decrease the efficiency of a system and in some cases even cause system failure.[6, 8]

Recently, NTE materials have garnered interest due to their potential use in composites with custom thermal expansion properties. As filler materials in composites, they can be used to reduce the overall thermal expansion without altering the characteristic properties of the original matrix. The preparation of composite

materials containing oxides that show NTE should allow control over the thermal expansion behavior and ideally avoid many limitations encountered from thermal expansion mismatches[10].

1.5.2 Negative thermal expansion in $A_2M_3O_{12}$

In recent years, the domains of microelectronics, optoelectronic communications, and aerospace have witnessed significant expansion. The rising demand for high-precision materials is evident, and the dimensional stability of devices over a range of operating temperatures is of high value[3].

A small change in thermal expansion coefficients, coupled with fluctuations in the environmental temperature of the materials, may induce thermal stress on the material . This can subsequently lead to a degradation in performance or even irreversible damage to the devices which can alter the performance and life of the device. Therefore , materials with low, and particularly near-zero, expansion are of great importance in enhancing the geometric stability of such materials and devices.

The recent discoveries in the field of negative thermal expansion (NTE) behavior in compounds has opened up the possibility of developing materials with adjustable or near-zero thermal expansion coefficients at operational temperature ranges , tailored for specific applications. This developments holds significant potential for improving the longevity and reliability of devices across various industries.

The $A_2M_3O_{12}$ ceramic family, where 'A' represents a trivalent cation ranging

from M^{6+} to M^{6+} , and 'M' typically signifies M^{6+} or M^{6+} , exhibits remarkable chemical versatility while maintaining a consistent fundamental crystal structure. Numerous members of this family demonstrate negative thermal expansion in one or more lattice vectors, resulting in atypical (near-zero, negative, or low-positive) thermal expansion coefficients. This unique property sets the $A_2M_3O_{12}$ ceramic family apart in the realm of materials science

The structure of $A_2M_3O_{12}$ is composed of one octahedron and one tetrahedron connected through a vertex. An asymmetric transverse vibration of the 2-fold oxygen is capable of contracting the A-M non-bonding distance and decreasing the A-O-M angle. The six crystallographically different A-O-M angles in orthorhombic $A_2M_3O_{12}$ are never equal to 180° , and their angles, which decrease with temperature, are between 140° and 175° . The peculiar lattice dynamics in the $A_2M_3O_{12}$ family, with the existence of many low-energy vibrational modes, has been confirmed by XRD diffraction data at different temperature ranges.

The crystal structure of $A_2M_3O_{12}$ exhibits a quasi two-dimensional configuration. The b-c layers are interconnected along the a-crystallographic direction (in the Pbcn space group) by a limited number of oxygen linkages per unit area. This is a unique characteristic, differing from the other two crystallographic directions. This structural peculiarity is mirrored in the lattice parameters, which display a diminished rigidity along the a-axis compared to the b and c axes. This elastic anisotropy diminishes as the Coefficient of Thermal Expansion (CTE) becomes increasingly negative, suggesting a correlation between the three-dimensional network-like behavior and Negative Thermal Expansion (NTE).

Generally, such a crystal framework induces NTE along the b and c directions, while the a-axis exhibits positive thermal expansion. This unique behavior underscores the complex interplay of structural and thermal properties in the $A_2M_3O_{12}$

crystal system.

1.5.3 Mechanism of NTE

Numerous oxide systems, composed of rigid polyhedra, exhibit Negative Thermal Expansion (NTE) behavior. These polyhedra are formed by a metal atom linked to several oxygen atoms via highly rigid bonds. The polyhedra are organized in corner-sharing frameworks, leaving substantial void space.[10]

In NTE materials, the metal-oxygen-metal (M-O-M) linkages of the polyhedra are nearly linear, with extremely rigid metal-oxygen bonds. Furthermore, the polyhedra show minimal changes in shape or size upon heating or cooling. When these materials are heated, transverse vibrations of the corner-sharing oxygens are more energetically favorable than longitudinal vibrations. This combination of transverse oxygen vibrations and rigid polyhedra results in coordinated tilting motions of the polyhedra upon heating, referred to as Rigid Unit Modes (RUMs).

During a RUM, polyhedra undergo a rocking motion, altering the distance between neighboring metals and consequently changing the overall volume of the system. The overall movement may result in either positive or negative thermal expansion, depending on the anharmonicity of the lattice vibrations.

Crystal structures consisting of face- or edge-sharing polyhedra typically do not exhibit NTE behavior, which can be attributed to the increased density of the unit cell. Unlike corner-sharing networks, edge- and face-sharing networks have little to no empty space around the polyhedra.[15]

The most well-known NTE oxides are from the zirconium tungstate (ZrW_2O_8) family. These compounds crystallize in a cubic unit cell and display the largest temperature range of isotropic NTE. Unlike other NTE materials that show shrinkage over a narrow temperature range, cubic ZrW_2O_8 exhibits negative thermal expansion from 83 K to 1050 K. The material undergoes a structural phase transition at 430 K, which is accompanied by a discontinuity in the expansion coefficient, but remains cubic both before and after the phase transition. During this transition, no bonds are broken or formed, only the bond angles change.[?]

1.5.4 Non-Hygrosopic

Hygrosopic tendencies in $\text{A}_2\text{M}_3\text{O}_{12}$ materials can lead to material degradation and can inhibit Negative Thermal Expansion (NTE). It has been observed that $\text{Yb}_2\text{M}_3\text{O}_{12}$ partially amorphizes in air at temperatures below 403 K, a behavior attributed to its hygrosopic nature. This hygrosopicity is also confirmed in all other tungstates and molybdates of the heavy rare earths from Lu to Ho.

In contrast, tungstates and molybdates of non-rare-earth A^{3+} cations, which possess smaller cationic radii, are not hygrosopic. The key structural characteristic that allows the entrance and accommodation of water molecules in the interior of the open orthorhombic $\text{A}_2\text{M}_3\text{O}_{12}$ -type structure is the presence of channels. These empty one-dimensional spaces are aligned along the c-axis directions. Their diameters are determined by the size of A^{3+} , and hence, smaller cations form narrow channels, which can inhibit water uptake.

Another explanation for the non-hygrosopic nature of tungstates and molybdates of smaller trivalent cations has been proposed based on a first-principles study. The chemical interactions between water molecules and the crystal frame-

work in the tungstate and molybdates of smaller A^{3+} are weaker, leading to lower absorption energies. As a result, these phases are resistant to humidity. Water molecules likely interact with the framework through hydrogen bonding. It has been suggested that oxygen atoms from water molecules interact with A^{3+} or M^{6+} , while hydrogen atoms from water molecules interact with 2-fold oxygens in the framework. These interactions between water molecules and the framework can cause amorphization in molybdates and tungstates or even change the crystal symmetry in some tungstates.

Symmetry lowering by transformation to the monoclinic phase, or the presence of water molecules in channels, will inhibit or attenuate the asymmetrical framework librations of the quasi-rigid polyhedra, due to freezing of polyhedra rocking motions or due to steric effects, respectively. Although zeolites neither amorphize in the hygroscopic form nor change symmetry, their NTE is inhibited unless totally dehydrated, proving that water molecules, or any other atom/molecule which occupies void spaces in the deficient garnet structure, will inhibit NTE. It is crucial to differentiate between hygroscopicity in molybdates and tungstates. Molybdates become amorphous when hygroscopic and lose water at temperatures higher than 303 K. Tungstates, however, lose water more readily, at temperatures not higher than 273 K and do not necessarily become amorphous. It has been proposed that differences in the hygroscopicity between tung states and molybdates are due to lower absorption energies of water molecules into the crystal framework in tung states.

There are two primary methods to reduce or inhibit the hygroscopicity in tungstates and molybdates. One is to partially substitute larger A^{3+} for smaller cations. The suppression of hygroscopic behavior has also been achieved by coating the hygroscopic $A_2M_3O_{12}$ material with a hydrophobic material.

CHAPTER 2 LITERATURE REVIEW

2 Review about $\text{Sc}_2\text{Mo}_3\text{O}_{12}$

2.1 A2M3O12 Family of Materials

The family of materials represented by the formula $\text{Sc}_2\text{Mo}_3\text{O}_{12}$ has been the subject of study due to its Negative Thermal Expansion (NTE) properties. These materials can be generalized by the formula $\text{A}_2\text{M}_3\text{O}_{12}$, where A represents a trivalent metal ranging in size from Al^{3+} to Dy^{3+} , and M is either W or Mo.

These compounds adopt the same orthorhombic structure as $\text{Sc}_2\text{W}_3\text{O}_{12}$, which they are named after. The compound $\text{Sc}_2\text{W}_3\text{O}_{12}$ was first reported in 1965, and its structure was later characterized as a network of corner-sharing ScO_6 octahedra and WO_4 tetrahedra.[1]

This family of materials is known to crystallize in a monoclinic P21/a or orthorhombic Pnca structure type. ““ This class of materials can display either Positive Thermal Expansion (PTE) or Negative Thermal Expansion (NTE), and covers a broad spectrum of thermal expansion coefficients from $\alpha_v = 37.2 \times 10^{-6} \text{ }^\circ\text{C}^{-1}$ to $\alpha_v = -34.5 \times 10^{-6} \text{ }^\circ\text{C}^{-1}$ for monoclinic $\text{In}_2\text{Mo}_3\text{O}_{12}$ and orthorhombic $\text{Ho}_2\text{Mo}_3\text{O}_{12}$, respectively.

These materials are capable of undergoing a reversible phase transition from an orthorhombic NTE phase at high temperatures to a monoclinic PTE structure at low temperatures. The monoclinic structure lacks the local symmetry required for NTE because the M-O-M bonds are not linear and deviate from 180° .

Certain compositions in this family exhibit NTE only within a limited temperature range. For instance, $\text{Fe}_2\text{Mo}_3\text{O}_{12}$ shows NTE with $\alpha_l = -14.82 \times 10^{-6} \text{ }^\circ\text{C}^{-1}$ between 550 and 800 $^\circ\text{C}$. On the other hand, $\text{Sc}_2\text{W}_3\text{O}_{12}$ demonstrates a larger than usual temperature range of NTE from -263 to 800 $^\circ\text{C}$ with an intrinsic

$$\alpha_l = -2.2 \times 10^{-6} \text{ } ^\circ\text{C}^{-1}.$$

2.2 Effect of A-site Cation on Properties

The A-site cation in $\text{A}_2\text{M}_3\text{O}_{12}$ materials influences the crystal structure and phase transition temperatures. Electronegative A-site cations can increase the phase transition temperature by reducing oxygen-oxygen repulsion, stabilizing the denser monoclinic structure. Most compositions transition from the monoclinic to the less dense orthorhombic phase at higher temperatures.

Certain materials in the scandium tungstate family, such as $\text{Y}_2\text{Mo}_3\text{O}_{12}$ and $\text{Y}_2\text{W}_3\text{O}_{12}$, do not undergo this phase transition. $\text{Dy}_2\text{W}_3\text{O}_{12}$ can crystallize in two polymorphs depending on thermal history. The monoclinic phase observed for slow-cooled samples differs from the typical P21/a structure observed in other $\text{A}_2\text{M}_3\text{O}_{12}$ materials.[2]

The C2/c phase is thermodynamically stable, while the orthorhombic Pnca phase is the stable high-temperature phase. Different polymorphs can be obtained by different heating protocols. The quenched material is hygroscopic and crystallizes in the trihydrate phase upon exposure to the atmosphere, which can be removed by heating above $180 \text{ } ^\circ\text{C}$.

Compositions with larger A-site cations generally display stronger NTEs because of larger, less rigid polyhedra. For example, $\text{Ho}_2\text{Mo}_3\text{O}_{12}$ has a volume thermal expansion coefficient of $-34.5 \times 10^{-6} \text{ } ^\circ\text{C}^{-1}$, while $\text{Al}_2\text{W}_3\text{O}_{12}$ possesses $\alpha_v = 6.6 \times 10^{-6} \text{ } ^\circ\text{C}^{-1}$.

2.3 Introduction to Methyl Orange Degradation

Methyl Orange (MO) is a widely used dye in various industries, and its release into the environment poses significant environmental challenges. The degradation

of MO has been a subject of intense study, with UV light-assisted degradation emerging as a promising technique. This process involves the use of UV light to break down the complex aromatic structure of the dye, making it less harmful to the environment.[2]

2.3.1 Mechanisms of UV Light-Assisted Degradation

The UV light-assisted degradation of MO can occur through two primary mechanisms: photolysis and photocatalysis. Photolysis refers to the process where MO degrades under UV light without the presence of a catalyst. Photocatalysis involves the use of a catalyst to enhance the degradation process. Studies have shown that photocatalysis can be more effective than photolysis in certain cases. For example, the use of nanostructured Ag / titania silica as a catalyst has been found to enhance the degradation of MO.[9]

2.3.2 Factors Influencing the Degradation Process

Several factors can influence the efficiency of the UV light-assisted degradation of MO. These include the nature and concentration of the catalyst, the initial concentration of MO, and the wavelength of the UV light. For example, experiments have shown that oxygen microbubbles can accelerate the decolorization rate of MO under specific UV light irradiation. Moreover, the use of doped catalysts, such as Mg-ZnO and Mn-ZnO nanocatalysts, has been found to significantly improve the degradation efficiency.[11, 5, 13]

CHAPTER 3 *EXPERIMENTAL*

3 Hydrothermal synthesis of $\text{Sc}_2\text{Mo}_3\text{O}_{12}$

In hydrothermal synthesis, reactants are heated in water/steam at high pressures and temperatures. The water acts as a pressure-transmitting medium and as a solvent. The solubility of the reactants is dependent on pressure and temperature. The reactants are placed in a Teflon-lined autoclave and heated in the oven. The autoclave maintains high temperature and pressure for the reaction to take place.

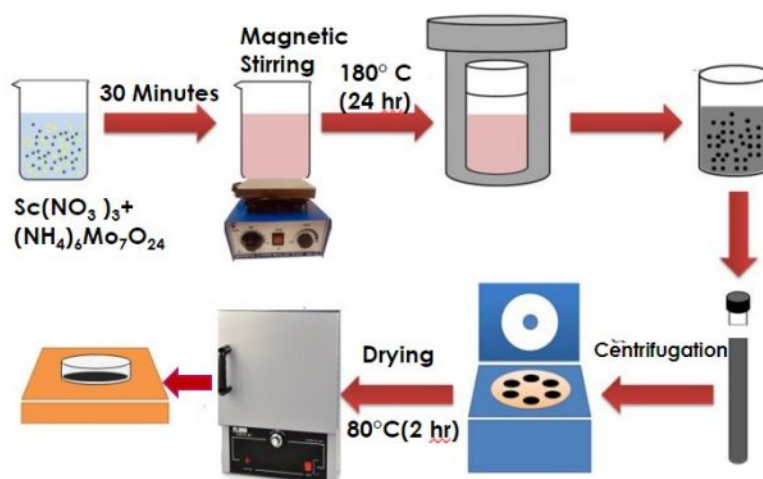


Figure 6: Hydrothermal synthesis process

3.1 Procedure

Stoichiometric amounts of $(\text{NH}_4)_6\text{MoO}_{24} \cdot \text{H}_2\text{O}$ and $\text{Sc}(\text{NO}_3)_3 \cdot \text{H}_2\text{O}$ were weighed and dissolved in a beaker containing 10 ml of Milli-Q water separately. Then the dopant were added to beaker that is $\text{Yb}(\text{NO}_3)_3 \cdot 6\text{H}_2\text{O}$ and $\text{Er}(\text{NO}_3)_3 \cdot 5\text{H}_2\text{O}$ according to their respective calculated weight. Then a magnetic stirrer was used to stir and dissolve the reactants for 20 minutes. $(\text{NH}_4)_6\text{MoO}_{24} \cdot 2\text{H}_2\text{O}$ solution was

poured into $Sc(NO_3)_3 \cdot H_2O$. The mixture was stirred again for 30 minutes. The neutral pH was maintained for the reaction. The mixture was made up to 40 ml by adding Milli-Q water and transferred to a Teflon lined autoclave, sealed, and kept in the oven for heating at $200^\circ C$ for 24 hours. The formed compound was washed, centrifuged several times with Milli-Q water, and dried. The final compound was formed after sintering at $800^\circ C$ for 2 hours. After the formation of compound to check its purity and composition it is perfectly grounded and transferred to pallet.

3.2 List of chemicals

For 0.2 grams of $Sc_{1.42}Mo_3O_{12} : 0.54Yb^{3+} : 0.04Er^{3+}$ we have used following compounds with respective mass as given below in table

Chemical Formula	Mass (grams)
$Sc(NO_3)_3 \cdot 6H_2O$	0.1551
$(NH_4)_6Mo_7O_{24} \cdot 4H_2O$	0.2338
$Yb(NO_3)_3 \cdot 6H_2O$	0.0812
$Er(NO_3)_3 \cdot 5H_2O$	0.00571

Table 1: Chemical Formulas and their Masses

For 0.2 grams of $Sc_{1.6}Mo_3O_{12} : 0.36Yb^{3+} : 0.04Er^{3+}$ we have used the following compounds with respective mass as given below in the table.

Chemical Formula	Mass (grams)
$Sc(NO_3)_3 \cdot 6H_2O$	0.1751
$(NH_4)_6Mo_7O_{24} \cdot 4H_2O$	0.2688
$Yb(NO_3)_3 \cdot 6H_2O$	0.0762
$Er(NO_3)_3 \cdot 5H_2O$	0.00587

Table 2: Chemical Formulas and their Masses

All chemicals were 99.99% pure and manufactured by Alfa Aesar.

3.3 Procedure for Degradation of Methyl orange

we have used $\text{Sc}_{1.42}\text{Mo}_3\text{O}_{12} : 0.54\text{Yb}^{3+} : 0.04\text{Er}^{3+}$ as a photocatalyst for the degradation of Methyl orange, first I have weighed 20 mg of $\text{Sc}_{1.42}\text{Mo}_3\text{O}_{12} : 0.54\text{Yb}^{3+} : 0.04\text{Er}^{3+}$ then transferred it to the beaker that contains 45 ml of ethanol and then we add 5 ml of the stock solution prepared earlier. The entire process takes around 15 minutes, then we have started the process, the initial step is to allow the compound to mix thoroughly with the solvent here its ethanol for exactly 1 hour. after 1 hour we set the UV lamp and took the first reading, this is our C0 reading at reference time 0 minutes, we repeated the entire process for 120 minutes until we got 12 readings. Then we took the dye degradation samples photo as a reference.

3.4 Procedure for XRD refinement

The Rietveld refinement and profile matching procedure for powder diffraction data involved following steps:

1. **Data Collection:** High-quality powder diffraction data is collected at ULMC at Goa university on the prepared ground sample with 2θ varying from 10° to 80° with a step size of 0.02° using Copper $K\alpha$ radiation. of wavelength 1.5408\AA since The quality of the data significantly impacts the reliability of the results.
2. **Phase Identification:** The collected diffraction pattern is compared with standard patterns in a Crystallographic open database to identify the phases present in the sample.
3. **Profile Matching:** The peak positions, intensities, and shapes in the diffraction pattern are matched to the standard patterns. This step provides an

initial estimate of the lattice parameters and crystallite size.

4. **Rietveld Refinement:** The initial model is refined by minimizing the difference between the observed and calculated diffraction patterns. The refinement process adjusts the parameters of the model, such as atomic positions, thermal parameters, and site occupancies, to best fit the observed data.
5. **Validation:** The quality of the refinement is assessed by examining the difference plot (observed - calculated), goodness-of-fit indicators, and reliability factors. If the refinement is not satisfactory, the model is revised, and the refinement is repeated.
6. **Result Interpretation:** The refined parameters are interpreted in terms of the crystal structure, lattice parameters, and phase present.

This procedure provides a comprehensive analysis of the crystallographic properties of a material from powder diffraction data. However, I carefully took data with Mahendra Sir in the chemistry department, model construction, and refinement gives as reliable results as discussed in last chapter.

CHAPTER 4 *CHARACTERISATION*

4 Characterisation of $\text{Sc}_2\text{Mo}_3\text{O}_{12}$

Characterization is a crucial step in developing high-quality materials. Examines a material's phase, structure, composition, microstructure, and spectroscopic properties. No single technique can provide a comprehensive characterization of a solid. This chapter describes the various analytical instruments employed to characterize the prepared samples.

The following instruments were used to characterize the phosphors.

1. X-ray diffractometer for XRD measurement
2. Structural analysis by Rietveld Refinement using Fullprof suit software.
3. Scanning electron microscope
4. Methyl orange degradation using sample

4.1 X-ray diffraction

X-ray diffraction (XRD) has been used for over a century to identify crystalline -phases as a fingerprint technique in the synthesis and structure determination.

4.1.1 Generation of X-rays

X-rays are electromagnetic waves with wavelengths of about $\approx 1\text{\AA}$. They are generated by accelerating high-energy electrons through a high-voltage field and colliding with a metal target. The resulting X-ray spectrum consists of two components: a continuous spectrum of varying wavelengths, called white radiation, and

a discrete spectrum of specific wavelengths, called characteristic radiation. X-ray diffractometers use monochromatic X-rays, which are selected from the characteristic radiation. When the electron beam hits the target, such as Cu, it can knock out electrons from the target atoms' innermost shell (K). This creates vacancies filled by electrons from higher shells (L, M), releasing energy as X-rays. The X-rays emitted by the transitions from L to K are called $K\alpha$ radiation, and those from M to K are called $K\beta$ radiation.

4.1.2 Interaction of X-rays with matter

Bragg's method of diffraction considers crystals to be composed of layers or planes, each functioning as a partially transparent mirror. When X-rays, whose wavelength is comparable to the distances between atoms, strike a crystal, some of the X-rays are reflected from the surface at an angle identical to the angle of incidence. The remaining X-rays pass through and are then reflected by subsequent layers.

Bragg's Law is given by:

$$2 * d \sin \theta = n\lambda \quad (1)$$

Where:

n is an integer,

λ is the wavelength of the incident radiation,

d is the spacing between crystal lattice planes,

θ is the angle of incidence.

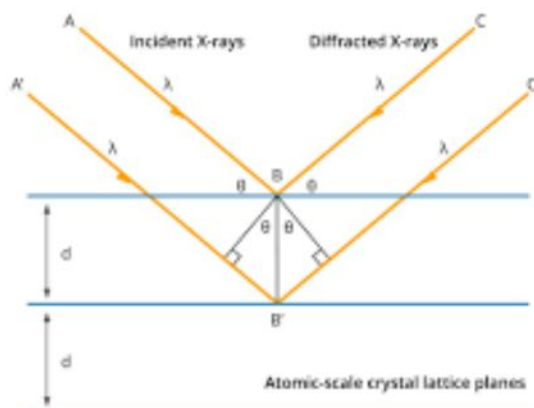


Figure 7: Schematic representation of Bragg's Law

When Bragg's law is satisfied, the reflected Bragg's are in phase and interfere constructively. For angles other than Bragg's angle, they are out of phase Bragg's interfere destructively. Bragg's law imposes strict conditions for reflection to occur.

4.2 Powder XRD method

A monochromatic X-ray beam is incident upon a finely powdered crystalline sample in this experimental setup. In the sample's random crystal orientation example, a subset of crystals oriented at the Bragg angle relative to the incident beam exists for any given set of lattice planes.

The diffracted beam is subsequently detected. Each set of lattice planes contributes to the diffraction pattern, with the diffracted radiation forming the surface of a cone. This phenomenon occurs because the requirement for diffraction is solely that the lattice planes are oriented at the Bragg angle to the incident beam, with no restrictions on the angular orientation of the planes about the incident beams.

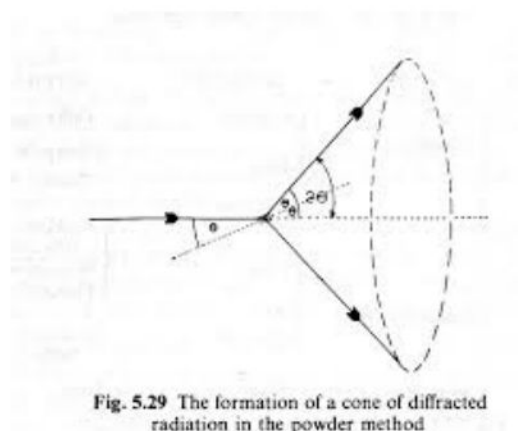


Figure 8: Formation of the cone of the diffracted beam.

4.2.1 Powder X-ray Diffractometer

A Powder X-ray Diffractometer comprises the following components:

X-ray Source: High-energy electrons are produced from a heated tungsten filament. These electrons are allowed to intrude on a small metal target, such as copper, in a sealed diffraction tube. **Collimator:** The X-rays generated by the target material pass through the collimator, which consists of two closely packed metal plates separated by a small distance. The collimator absorbs all X-rays except for the narrow beam that passes through it. **Monochromators:** Monochromators separate polychromatic light into a range of individual wavelengths. A Graphite Monochromator, used in the Rigaku Smart Lab X-ray diffractometer, optimizes sensitivity by lowering the background level. It improves the signal-to-noise ratio by eliminating fluorescence from materials containing Co, Ni, Fe, and Mn. **Filters:** Filters absorb undesirable radiation, but allow radiation of the desired wavelength to pass. For example, a nickel filter removes $K\beta$ radiations of copper. These filters are used as an alternative to monochromators. **Detector:** The D/TEX Ultra 250 detects the diffracted beam in the Rigaku Smart Lab powder X-ray diffractometer. It is a 1D silicon strip detector that decreases data acquisition time by 50% com-



Figure 9: Rigaku Smart Lab Powder X-ray diffractometer at ULMC of Goa University

pared to competitive detectors. This is achieved by increasing the active area of the aperture, thus increasing the count rate. The D/TAX Ultra has a smaller pixel pitch and is longer in the direction of 2θ .



Figure 10: Rigaku Smart Lab Powder X-ray diffractometer at ULMC of Goa University

4.3 Scanning Electron Microscopy

Scanning electron microscopes are among the most versatile or multifaceted instruments. They are used to observe structure morphology at higher magnification and to characterize chemical composition.

4.3.1 Principle

A Scanning Electron Microscope (SEM) operates on the principle of utilizing kinetic energy to generate signals from electron interactions. These electrons can be categorized into three types: secondary electrons, back-scattered electrons, and diffracted back-scattered electrons. These categories of electrons play a crucial role in visualizing crystallized elements and photons.

Back-scattered Electrons: Back-scattered electrons are reflected when the primary electron beam interacts with the sample. These interactions are elastic.

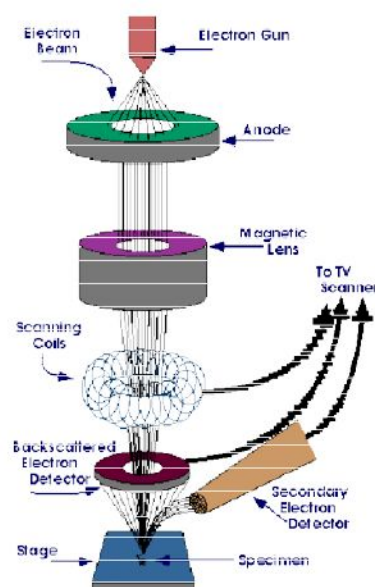


Figure 11: Schematic diagram of a Scanning electron microscope

Back-scattered electrons originate from deeper areas within the samples. The images produced by these electrons display high sensitivity to differences in atomic numbers, which are represented as variations in brightness.

Secondary Electrons: Secondary electrons are emitted from the atoms of the sample and are involved in inelastic interactions. These electrons originate from the surface regions of the sample. The scattered electrons provide information about the nano and microstructure of the samples, represented in the form of an image.

Scintillator: A scintillator is used as a detector, which is maintained at a high positive potential of several kilovolts. The secondary electrons are accelerated into the scintillator, producing visible light, which is then detected by a photomultiplier.

Signals are emitted and collected by detectors at each point on the specimen. The detector signal is synchronized with the known location of the beam on the specimen, and the signal intensity is used to modulate the corresponding image

pixel. The signals collected in series are combined to form an image, the dimensions of which depend upon the chosen scan pattern.

4.3.2 Instrumentation

A Scanning Electron Microscope (SEM) consists of the following components:

Electron Source: The electron source at the top of the microscope column generates electrons. These electrons are emitted by a heated filament of Tungsten through thermionic emission.

Anode: The anode carries a positive charge, attracting the electrons to form an electron beam.

Magnetic Lens: The magnetic lens controls the size of the beam and determines the number of electrons in the beam. The size of the beam dictates the resolution of the image. Apertures can also be used to control the size of the image.

Scanning Coils: The scanning coils deflect the electrons along the x and y axes, ensuring that the beam scans over the sample's surface in a raster pattern.

Objective Lens: The objective lens is the final lens that shapes the electron beam. As this lens is very close to the sample, it focuses the beam to a tiny spot on the sample.

Since electrons cannot pass through glass, SEM lenses are electromagnetic. They are composed of a coil of wire inside metal poles. When current passes through these coils, they generate a magnetic field. Since electrons are highly sensitive to magnetic fields, the lenses in the microscope can control them.

4.3.3 Application

The primary application of Scanning Electron Microscopy (SEM) lies in the high-resolution examination of materials. SEM provides detailed information about



Figure 12: Carl Zeiss Scanning Electron Microscope at ULMC of Goa University

solid surface sizes, shapes, and compositions. The results obtained from SEM complement those derived from optical microscopy by offering insights into features at the submicron level. However, the scope of SEM extends to features spanning hundreds of microns.

Images can be recorded using both secondary electrons and backscattered electrons. The instrumental conditions are optimized to yield excellent topographic contrast. This dual-mode imaging capability enhances the versatility of SEM, enabling comprehensive surface analysis that encompasses fine and coarse features. Thus, SEM serves as a powerful tool in materials science, facilitating in-depth characterization of a wide range of materials.

CHAPTER 5 *ANALYSIS AND CONCLUSIONS*

5 Analysis of $\text{Sc}_2\text{Mo}_3\text{O}_{12}$

5.1 XRD Refinement

The Powder XRD data on finely grounded samples was taken at ULMC at Goa university. The both compounds are orthorhombic in nature as obtained from PXRD analysis by Reitveld refinement by using Fullprof software. We followed the procedure described in Chapter 2 for refinement. The lattice constants and phase of the compound are the conclusion derived from the experiment. The lattice constants and chi factor values along with a graphical representation of the observed and calculated measurements are provided below.

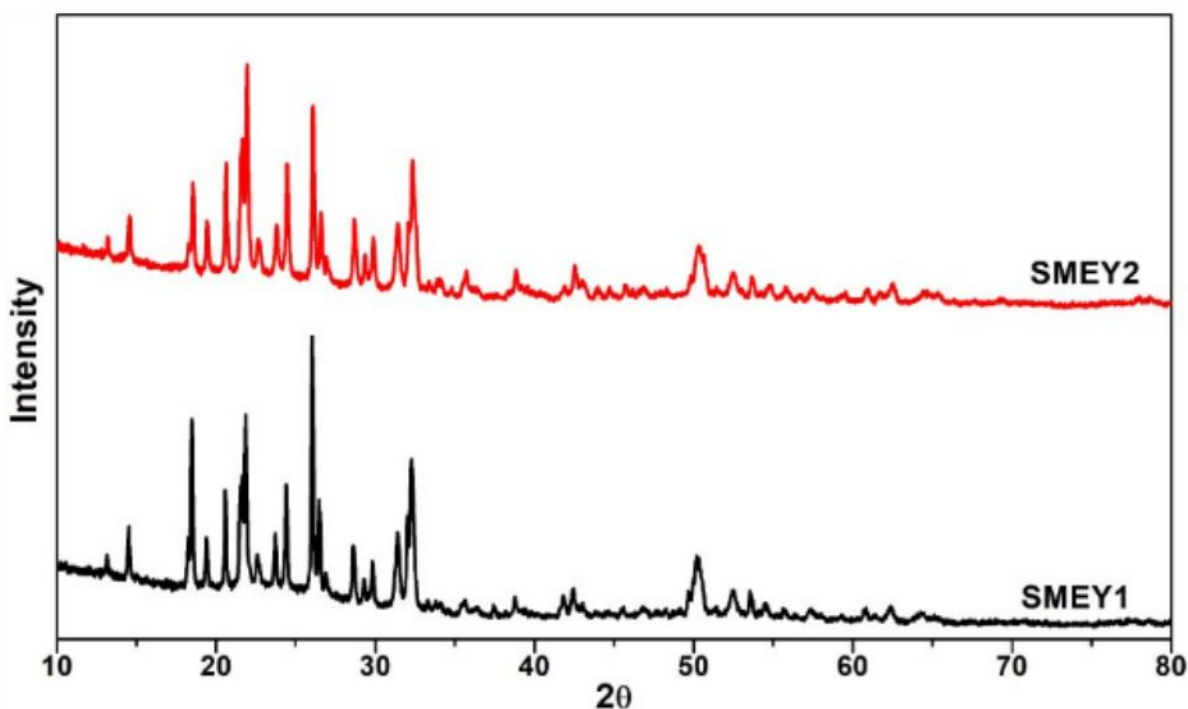


Figure 13: XRD plot of both samples

The refinement of each sample is performed afterwards as below

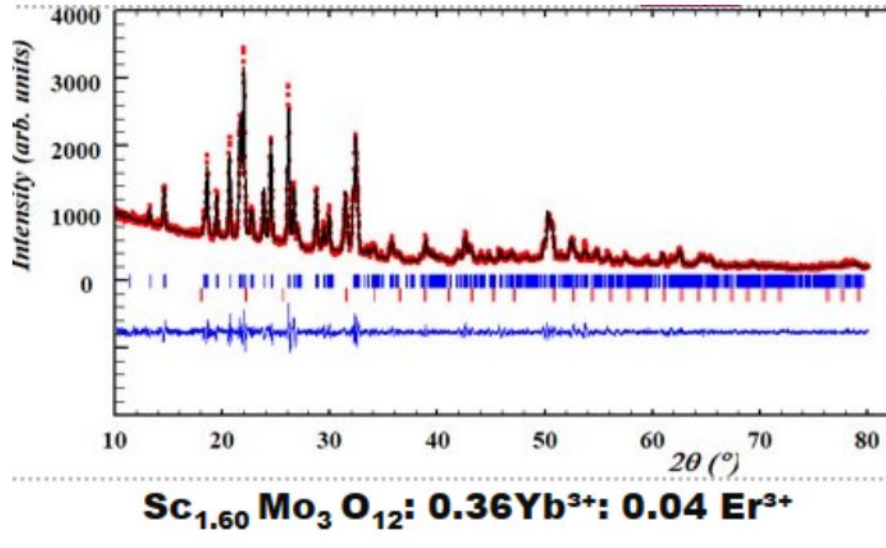


Figure 14: $\text{Sc}_{1.6}\text{Mo}_3\text{O}_{12} : 0.36\text{Yb}^{3+} : 0.04\text{Er}^{3+}$

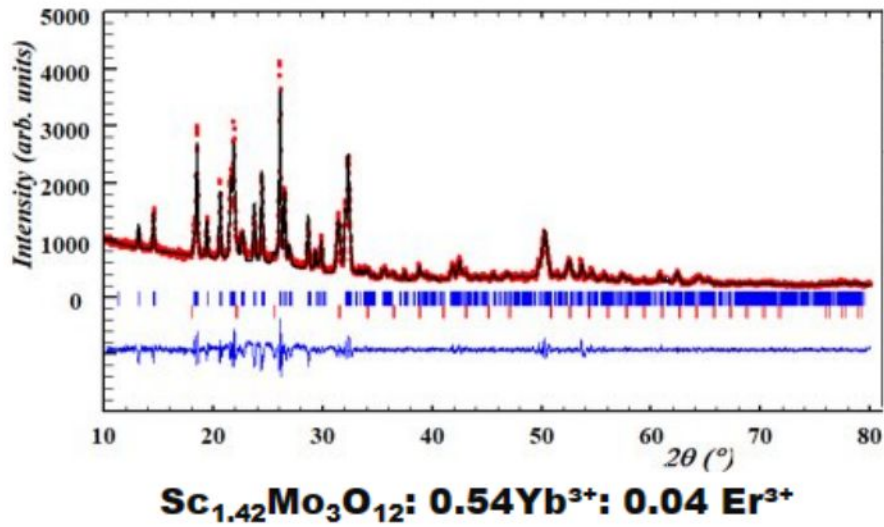


Figure 15: $\text{Sc}_{1.42}\text{Mo}_3\text{O}_{12} : 0.54\text{Yb}^{3+} : 0.04\text{Er}^{3+}$ refinement

The discription of lattice parameters are given as below in tabular format

Compound	a	b	c	χ^2
Sc _{1.42} Mo ₃ O ₁₂ : 0.54Yb ³⁺ : 0.04 Er ³⁺	9.7049	13.4237	9.5908	3.04
Sc _{1.60} Mo ₃ O ₁₂ : 0.36Yb ³⁺ : 0.04 Er ³⁺	9.6778	13.3494	9.57133	2.28

Table 3: Lattice parameters for samples.

5.2 SEM analysis

The SEM images give as clear idea about surface topology of our sample both samples having irregular topography with sizes ranging from 2 micron to 8 micron. The images were taken from the Department of Electronics Studies of Goa University. The images are given below

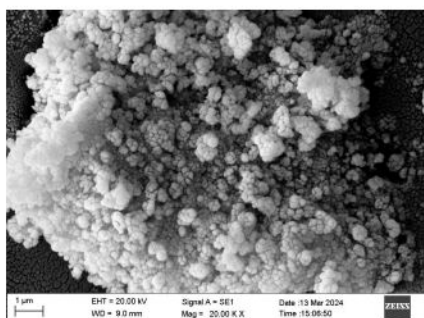


Figure 16: Sc_{1.42}Mo₃O₁₂ : 0.54Yb³⁺ : 0.04Er³⁺

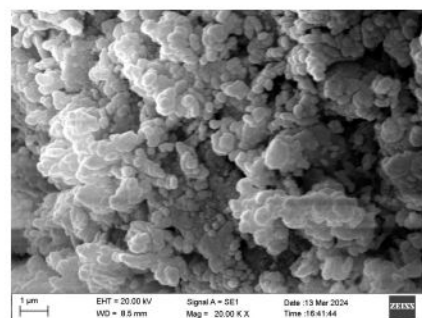


Figure 17: Sc_{1.6}Mo₃O₁₂ : 0.36Yb³⁺ : 0.04Er³⁺

5.3 UV degradation

The application of our compound Sc_{1.42}Mo₃O₁₂ : 0.54Yb³⁺ : 0.04Er³⁺ can be seen in the degradation of methyl orange. we have used the compound as a photocatalyst.

First we have used Sc_{1.42}Mo₃O₁₂ : 0.54Yb³⁺ : 0.04Er³⁺ as a photocatalyst for the degradation of Methyl orange, first I have weighed 20 mg of Sc_{1.42}Mo₃O₁₂ :

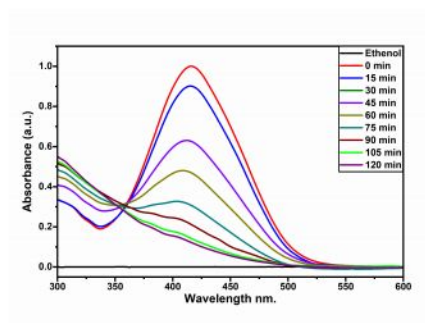


Figure 18: Graph of Absorbance vs Wavelength.

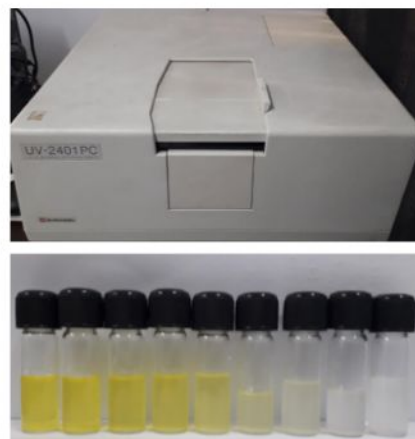


Figure 19: UV recording spectrometer and degraded MO

$0.54\text{Yb}^{3+} : 0.04\text{Er}^{3+}$ and then transferred it to the beaker that contains 45 ml of ethanol and then we add 5 ml of the stock solution prepared earlier. The entire process takes around 15 minutes, then we have started the process, the initial step is to allow the compound to mix thoroughly with the solvent here its ethanol for exactly 1 hour. after 1 hour we set the UV lamp and took the first reading, this is our C0 reading at reference time 0 minutes, we repeated the entire process for 120 minutes until we got 12 readings. Then we took the dye degradation samples photo as a reference.

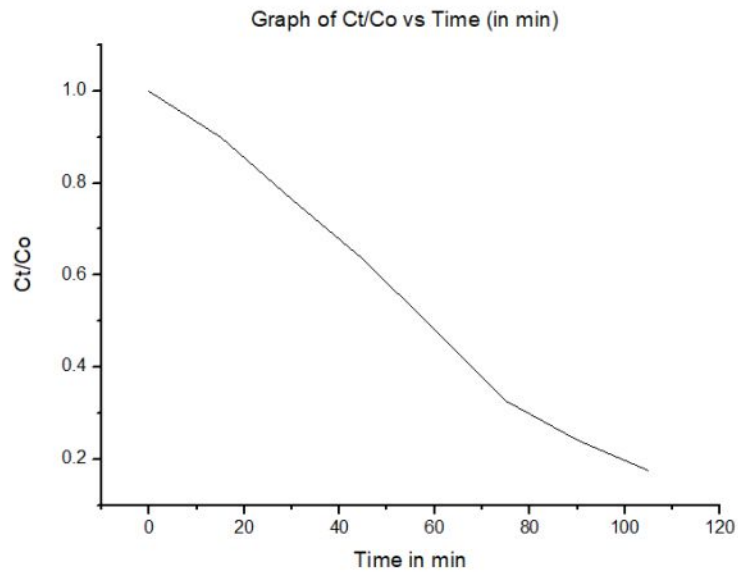


Figure 20: Graph of Ct/Co vs Time for $\text{Sc}_{1.42}\text{Mo}_3\text{O}_{12} : 0.54\text{Yb}^{3+} : 0.04\text{Er}^{3+}$

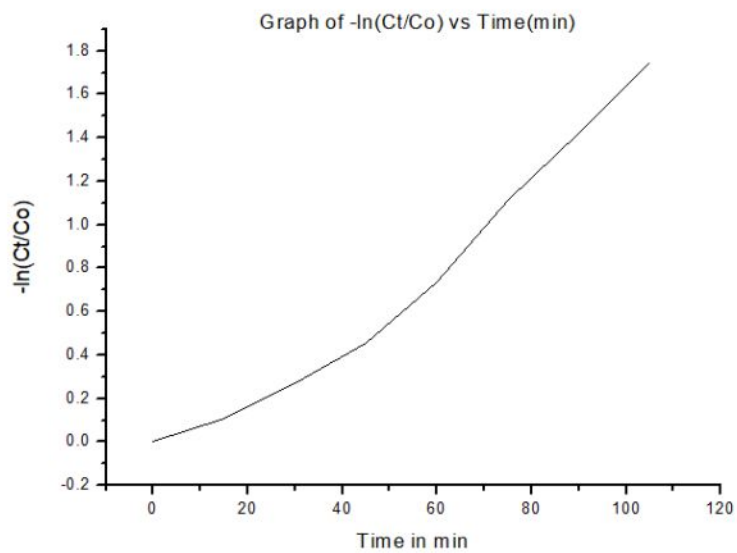


Figure 21: Graph of $-\ln(\text{Ct}/\text{Co})$ vs Time for $\text{Sc}_{1.42}\text{Mo}_3\text{O}_{12} : 0.54\text{Yb}^{3+} : 0.04\text{Er}^{3+}$

References

- [1] A. Ajmal, I. Majeed, R. N. Malik, H. Idriss, and M. A. Nadeem. Principles and mechanisms of photocatalytic dye degradation on tio 2 based photocatalysts: a comparative overview. *Rsc Advances*, 4(70):37003–37026, 2014.
- [2] S. Al-Qaradawi and S. R. Salman. Photocatalytic degradation of methyl orange as a model compound. *Journal of Photochemistry and photobiology A: Chemistry*, 148(1-3):161–168, 2002.
- [3] G. Blasse, B. Grabmaier, G. Blasse, and B. Grabmaier. Lamp phosphors. *Luminescent Materials*, pages 108–133, 1994.
- [4] L. Bøtter-Jensen. Luminescence techniques: instrumentation and methods. *Radiation Measurements*, 27(5-6):749–768, 1997.
- [5] S. Haji, B. Benstaali, and N. Al-Bastaki. Degradation of methyl orange by uv/h₂o₂ advanced oxidation process. *Chemical Engineering Journal*, 168(1):134–139, 2011.
- [6] F. Jahanbazi and Y. Mao. Impact of negative thermal expansion on thermal quenching of luminescence of sc₂mo₃o₁₂: Eu³⁺. *Chemistry of Materials*, 34(23):10538–10547, 2022.
- [7] C. C. Klick and J. H. Schulman. Luminescence in solids. In *Solid state physics*, volume 5, pages 97–172. Elsevier, 1957.
- [8] J. Li, X. N. Cheng, and J. J. Zhu. Preparation of sc₂mo₃o₁₂ and characterization of its negative thermal expansion property. *Applied Mechanics and Materials*, 320:181–184, 2013.

- [9] Y. Li, X. Li, J. Li, and J. Yin. Photocatalytic degradation of methyl orange by tio₂-coated activated carbon and kinetic study. *Water research*, 40(6):1119–1126, 2006.
- [10] H. Liu, N. Zhang, and Z. Zhang. Investigating negative thermal expansion property of decahedral sc₂mo₃o₁₂ prepared via hydrothermal method. *Solid State Sciences*, 132:106961, 2022.
- [11] H. Ma, B. Wang, and X. Luo. Studies on degradation of methyl orange wastewater by combined electrochemical process. *Journal of hazardous materials*, 149(2):492–498, 2007.
- [12] K. Murthy and H. S. Virk. Luminescence phenomena: an introduction. In *Defect and diffusion forum*, volume 347, pages 1–34. Trans Tech Publ, 2014.
- [13] Y. Sha, I. Mathew, Q. Cui, M. Clay, F. Gao, X. J. Zhang, and Z. Gu. Rapid degradation of azo dye methyl orange using hollow cobalt nanoparticles. *Chemosphere*, 144:1530–1535, 2016.
- [14] D. Vij. *Luminescence of solids*. Springer Science & Business Media, 2012.
- [15] D. T. Vu, Y.-C. Tsai, Q. M. Le, S.-W. Kuo, N. D. Lai, H. Benisty, J.-Y. Lin, H.-C. Kan, and C.-C. Hsu. A synergy approach to enhance upconversion luminescence emission of rare earth nanophosphors with million-fold enhancement factor. *Crystals*, 11(10):1187, 2021.
- [16] F. E. Williams and H. Eyring. The mechanism of the luminescence of solids. *The Journal of Chemical Physics*, 15(5):289–304, 1947.
- [17] H. Zou, B. Chen, Y. Hu, Q. Zhang, X. Wang, and F. Wang. Simultaneous enhancement and modulation of upconversion by thermal stimula-

tion in $\text{Sc}_2\text{Mo}_3\text{O}_{12}$ crystals. *The Journal of Physical Chemistry Letters*, 11(8):3020–3024, 2020.